# FLUID-STRUCTURE INTERACTION OF CYLINDERS BY COMBINING THE COSSERAT BEAMS THEORY AND IMMERSED BOUNDARY METHODOLOGY

**João Marcelo Vedovoto, jmvedovoto@mecanica.ufu.br**
**Felipe Pamplona Mariano, fpmariano@mecanica.ufu.br**
**Aristeu da Silveira Neto, aristeus@mecanica.ufu.br**
**Domingos Alves Rade, domingos@ufu.br**
Universidade Federal de Uberlândia - UFU
Faculdade de Engenharia Mecânica - FEMEC
Av: João Naves de Ávila, 2121
Campus Santa Mônica, Bl: 5P
CEP: 38400-902 Uberlândia-MG-Brasil
Phone:+55 (34) 3239-4040 / Fax:+55 (34) 3239-4042

**Adailton Silva Borges, adailton@utfpr.edu.br**
Universidade Tecnológica Federal do Paraná – UTFPR
Departamento de Engenharia Mecânica
Av. Alberto Carazzai, 1640
Campus Cornélio Procópio
CEP 86300-000 - Cornélio Procópio – PR
Phone: +55 (43) 3520-4000 / Fax: +55 (43) 3520-4010

***Abstract.*** *A fully coupled simulation of three dimensional problems involving fluid structure interactions is the most accurate way to predict the behavior of high aspect ratio cylinders in cross flows. The main interest in this kind of flows are due the great number of applications in the oil and gas industry (especially as related to the modeling of risers used for oil exploitation in deep seas), however there are inherent difficulties in the simulation of the fluid structure interaction of long and thin cylinders, as examples the high computational cost due the fact that a cylinder is moving across the computational domain associated with the necessity of the structural model be able to deal with high displacements.*
*In this work we circumvent these difficulties by the joint of two methodologies: the combination of the Cosserat theory applied to slender beams, and the Immersed Boundary methodology, which is used to represent the interactions between the structural and fluid domains. The main features of the proposed methodology are evaluated by means of a number of numerical simulations, both in static and dynamic regimes, regarding the structural model, in a first step and the complete fluid-structure model, in a second step. The results obtained enable to evaluate the accuracy and the main advantages and shortcomings of the methodology, especially regarding the numerical aspects. Also, they enabled to put in evidence some relevant phenomenological aspects related to the dynamic behavior of cylindrical structures with various levels of bending flexibility, subjected to transverse flows characterized by different values of the Reynolds number.*

***Keywords****: Fluid Structure Interaction, Vortex Induced Vibration, Immersed Boundary Method, Cosserat Theory.*

## 1. INTRODUCTION

The flow past a cylindrical structure can be the source of vibrations generated by vortex shedding. Such vibrations can induce to an increase of the drag coefficient, thus leading to an increase of the efforts over structure. The vibrations can lead also to the failure of a structure due fatigue. This is especially important when these cylinders are risers of oil exploitation subject to waves and/or maritime currents. According to Baarholm et al. (2006), two approaches have been adopted for solving fluid-structure interactions (FSI): empirical models and methodologies based on numerical simulation of governing equations (for both fluid and structure)

The present work describes the research work carried-out with the aim of developing, implementing and evaluating a three-dimensional modeling procedure of fluid-structure phenomena involving slender structures, such as beams, bars and cables. The novel approach adopted consists of the combination of the Cosserat theory (Argyris et al., 1978) applied to slender beams, which accounts for geometrical nonlinearity, and the Immersed Boundary methodology (Lima e Silva et al., 2003), which is used to represent the interactions between the structural and fluid domains. The study is included in the scope of Vortex-Induced Vibrations, which is a topic of great interest in the oil industry, especially as related to the modeling of risers used for oil exploitation in deep seas. According to the Cosserat theory, the deformed configuration of the structure is described in terms of the displacement vector of the curved formed by the cross-sections center of area, and

the orientation of a vector bases fixed to each cross-section, with respect to an inertial reference frame. The main advantage of this theory is that is geometrically exact. The finite element method is employed for discretization of the equations of motion for the structure.

Through the Immersed Boundary methodology, the solid-fluid interface forces are evaluated by enforcing momentum to the fluid particles over the interface fluid-solid. Such a methodology is particularly suitable for problems involving fluid-structure interactions, once the difficulty of re-meshing the computational grid is circumvented by the use of two independent domains. The governing equations of fluid flow are solved in an Eulerian domain (fixed, cartesian for instance), while the immersed geometry (or geometries) is (are) represented by a set of Lagrangian points. The coupling between both domains is made by the utilization of interpolation/distribution functions, which are based on discrete versions of a Dirac delta function.

The main features of the proposed methodology are evaluated by means of a number of numerical simulations, both in static and dynamic regimes, regarding the structural model, in a first step and the complete fluid-structure model, in a second step. The results obtained enable to evaluate the accuracy and the main advantages and shortcomings of the methodology, especially regarding the numerical aspects. Also, they enabled to put in evidence some relevant phenomenological aspects related to the dynamic behavior of cylindrical structures with various levels of bending flexibility, subjected to transverse flows characterized by different values of the Reynolds number.

## 2. Mathematic modeling for FSI

The FSI numerical approach adopted is named partitioned, *i.e.* in the same time step (Δt) the coupling between the fluid and the structure is separated in two parts, first it is solved the transport and conservation equations of the fluid medium (Navier-Stokes equations), after that the equations for the motion of the structure equations (Cosserat Theory) are solved, as is shown in Figure 1.

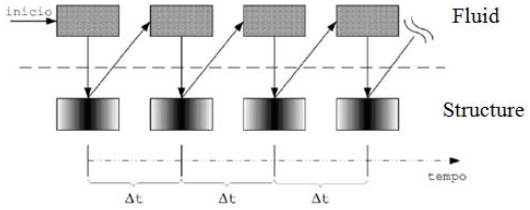


Figure 1. Partitioned approach for FSI.

The follow sections provide the detail of the formulation retained for the fluid, structure and the coupling between.

### 2.1. Mathematic model for the fluid

The flow is governed by conservation momentum equation (Eq. 1) and the continuity equation (Eq. 2). The information of the fluid/solid interface (domain $\Gamma$) is passed to the eulerian domain ($\Omega$) for addition of the term source to Navier-Stokes equations. This term plays a role of a body force that represents the boundary conditions of the immersed geometry. The equations that govern the problem are presented in theirs tensorial form:

$$\frac{\partial \rho u_i}{\partial t} + \frac{\partial (\rho u_i u_j)}{\partial x_j} = -\frac{\partial p}{\partial x_i} + \frac{\partial}{\partial x_j}\left[\mu\left(\frac{\partial u_i}{\partial x_j} + \frac{\partial u_j}{\partial x_i}\right)\right] + f_i, \tag{1}$$

$$\frac{\partial u_j}{\partial x_j} = 0, \tag{2}$$

where $p$ is the static pressure; $u_i$ are the velocity, $f_i$ are the IB term source in, $\rho$ is the density, μ is the kinematic viscosity; $x_i$ and $t$ are the spatial component the time respectively.

The algorithm under consideration for the simulation of the fluid motion is based on a classical predictor-corrector time integration scheme that employs a projection method for the momentum equations. The finite volume spatial discretization of the Navier-Stokes equations (N-S equations henceforth) is based on a staggered framework with velocity and scalar quantities evaluated in different grids to avoid the rise of checkerboard pressure patterns. Regarding the temporal integration of the N-S equations, the schemes retained are essentially controlled by the Courant criterion $Co = (u_i \Delta t)/\Delta x;\ u = 1, 2, 3$.

Explicit schemes exhibit numerical stability issues when using Courant number values larger than unity. However, such a numerical limitation does not apply to implicit or semi-implicit discretizations. The temporal integration schemes retained in the present work are fully implicit, in such a manner that it is possible to reach statistically steady regimes faster than by resorting to explicit time integration techniques (Vedovoto, 2009). To ensure regarding the robustness of a numerical method for solving the problems of interest, another important aspect analyzed in this revision is the choice of the temporal integration scheme. Here, besides the use of an fully implicit scheme permitting the use that allows to reach statistically steady regimes faster than by resorting to explicit time integration techniques, we show a formulation that allows the use of different methods of temporal integration, e.g. the Crank Nicolson method, a modified Crank Nicolson method, the Leap Frog and the backward difference formula methods.

The source term $f_i$, defined in all domain $\Omega$, is null, excepting the regions where the control volumes coincide with the immersed geometry, enabling the Eulerian field to perceive the presence of solid interface. Eq. (3) displays its behavior.

$$f_i(\vec{x},t)=\begin{cases} F_i(\vec{x}_k,t) & \text{if } \vec{x}=\vec{x}_k \\ 0 & \text{if } \vec{x}\neq\vec{x}_k \end{cases}, \tag{3}$$

where $\vec{x}$ is the position of the particle in the fluid and $\vec{x}_k$ is the position of a point in solid interface, (Mariano *et al.* 2010).

Through Eq. (3) it is possible to conclude that the field $f_i(\vec{x},t)$ is discontinuous, and hence can be evaluated only when there is a coincidence between the points that compose the interface immersed boundary-fluid domain. It is rarely the case when there is a coincidence between the Lagrangian points and the control volumes. If a staggered framework of discretization is retained for the fluid equations, such a coincidence never happens once the primary variables of the fluid are positioned in different locations. When the flows of interest have complex geometries within the computational domain ($\Omega$) it is necessary to distribute the function $f_i(\vec{x},t)$ on its neighborhoods. This is achieved by replacing the Dirac delta function by a discrete interpolation/distribution function. There are numerous forms of such a function. A detailed study of the form and efficiency of then can be found in Griffith and Peskin, (2005).

### 2.2. Mathematic model for the immersed interface

The lagrangian force field is evaluated by the direct forcing methodology, which was proposed by Uhlmann (2005). One of the characteristics of this model is that *ad-hoc* constants are not necessary; therefore the modeling of non-slip condition on immersed interface is physically more consistent. The Lagrangian force $F_i(\vec{x}_k,t)$ on the point *k* is evaluated by a balance of momentum over a particle of fluid coincident with the fluid-solid interface:

$$F_i(\vec{x}_k,t)=\frac{\partial \rho u_i}{\partial t}(\vec{x}_k,t)+\frac{\partial}{\partial x_j}(\rho u_i u_j)(\vec{x}_k,t)+\frac{\partial p}{\partial x_i}(\vec{x}_k,t)-\frac{\partial}{\partial x_j}\left[\mu\left(\frac{\partial u_i}{\partial x_j}+\frac{\partial u_j}{\partial x_i}\right)\right](\vec{x}_k,t). \tag{4}$$

The values of $u_i(\vec{x}_k,t)$ and $p(\vec{x}_k,t)$ are provided by interpolating of velocities and pressure respectively from Eulerian values of control volumes near the immersed interface. For the Lagrangian point $x_k$ at the immersed boundary, we have:

$$F_i(\vec{X}_k,t)=\frac{u_i(\vec{x}_k,t+\Delta t)-u_i^*(\vec{x}_k,t)+u_i^*(\vec{x}_k,t)-u_i(\vec{x}_k,t)}{\Delta t}+RHS_i(\vec{x}_k,t), \tag{5}$$

where $u^*$ is a temporary parameter (Wang, *et al.* 2008) and $RHS_i(\vec{x}_k,t)$. Is the sum of the advective, pressure and diffusive contributions of Eq. (5). The latter equation is decomposed and solved by Eqs. (6) and (7) in same time step:

$$\frac{u_i^*(\vec{x}_k,t)-u_i(\vec{x}_k,t)}{\Delta t}+RHS_i(\vec{x}_k,t)=0, \tag{6}$$

$$F_i(\vec{x}_k,t)=\frac{u(\vec{x}_k,t+\Delta t)-u_i^*(\vec{x}_k,t)}{\Delta t}, \tag{7}$$

where $u(\vec{x}_k,t+\Delta t)=U_{FI}$ is the immersed boundary velocity at the interface.

Equation (6) is solved on the Eulerian domain by the methods described in the section of mathematical and numerical methods for solving the fluid governing equations. $u_i^*(\vec{x},t)$ is interpolated for Lagrangian domain, became $u_i^*(\vec{x}_k,t)$ and it is computed on Eq. (7). Then $F_i(\vec{x}_k,t)$ is smeared on the Eulerian grid. Finally, the velocity is update by Eq. (8):

$$u_i(\vec{x},t+\Delta t) = u_i^*(\vec{x},t) + \Delta t.f_i. \tag{8}$$

### 2.3. Mathematic model for structure

One of the most important features of this theory is how the beam is spatially defined in terms of movement of the line passing through their cross sections centroids, defined by the vector $\boldsymbol{r}(s,t)$in a Cartesian fixed (inertial) base represented by $F = \{\boldsymbol{e}_1, \boldsymbol{e}_2, \boldsymbol{e}_3\}$ with unit vectors $\boldsymbol{e}_i$, and a set of orthogonal unit vectors attached to the cross section, forming the basis $S = \{\boldsymbol{d}_1(s,t), \boldsymbol{d}_2(s,t), \boldsymbol{d}_3(s,t)\}$, where the variable $S$ represents the position of the cross section along the line of centroids. Therefore, for each point on the curve formed by the centroids there is a orthonormal moving frame, formed by the unit vector $\boldsymbol{d}_i(s,t)$, that are defined externally to the position vector $\boldsymbol{r}(s,t)$. In Figure 2) we have the schematic representation of a segment of Cosserat beam, which are represented in the two bases mentioned previously.

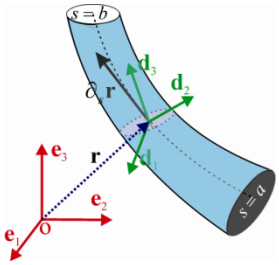


Figure 2. Schematic model of an element of Cosserat.

For convenience, we adopt that $\boldsymbol{d}_1(s,t)$ and $\boldsymbol{d}_2(s,t)$ are contained in the plane of cross section and, consequently, $\boldsymbol{d}_3(s,t)$ results perpendicular to that plane.

According to the beam theory of Cosserat, the strain are classified in two groups: linear strain **v**(s) and angular strain **u**(s). The components $\mathbf{v}_1$(s) and $\mathbf{v}_2$(s) are called shear strain and $\mathbf{v}_3$(s) is named elongation. While $\mathbf{u}_1$(s) and $\mathbf{u}_2$(s) are described as bending strain, $\mathbf{u}_3$(s) is called the torsion strain.

The relationship between linear and angular deformation, which is subject to a segment of Cosserat beam, and the fixed and moving bases is established to provide a complete description, that is, the spatial position of the centroids as the rotation of the cross-section. Thus the vector of linear deformation is given in terms of torsion angles and rotation of the cross section, and these relations are used later in the dynamic analysis. In this work we chose to omit these deductions but the mathematical details are found in the work of Borges (2010).

#### 2.3.1. The governing equations of motion

The local dynamic behavior of a beam element of Cosserat with density $\rho(s)$ and cross-sectional area *A(s)*, as shown by Antman (1995), is given by partial differential equations:

$$\frac{\partial \mathbf{h}(s,t)}{\partial t} = \frac{\partial \mathbf{m}(s,t)}{\partial s} + \mathbf{v}(s,t)\times\mathbf{n}(s,t) + \mathbf{l}(s,t) \tag{9}$$

$$\rho(s)A(s)\frac{\partial^2 \mathbf{r}(s,t)}{\partial t^2} = \frac{\partial \mathbf{n}(s,t)}{\partial s} + \mathbf{f}(s,t) \tag{10}$$

It is observed that Eqs (3.24) - (3.25) are resulting from the application of the principles of Newton-Euler differential element of the beam. In these equations, $\boldsymbol{n}(s,t)$, $\boldsymbol{m}(s,t)$, $\boldsymbol{h}(s,t)$, $\boldsymbol{f}(s,t)$ and $\boldsymbol{I}(s,t)$ are respectively the contact force, the contact moment (internal), the angular momentum, the external force and external moment, all per unit of length.

In the Cosserat theory of beams, unlike the classical theory of beams discretized by the method of finite elements, the shape functions can be obtained from differential equations of static equilibrium, and therefore take into account all the nonlinearities of system. As a consequence, we can increase the precision of the dynamic response by dividing the structure into a few elements, whose number is usually much smaller than traditional methods of finite elements. However, the advantage provided by the Cosserat theory is obtained at the cost of more complex analytical and numerical procedures.

The shape functions of the beam, depending on the nodal displacements and rotations, are obtained from solving the equation of static equilibrium. In literature, the static equilibrium is understood as the absence of external forces, and from Eq. (10), is that the contact forces shall meet:

$$\frac{d\mathbf{n}(s)}{ds} = 0 \tag{11}$$

And yet, from Eq. (9), the contact moments satisfy:

$$\frac{d\mathbf{m}(s)}{ds} + \mathbf{v}(s) \times \mathbf{n}(s) = 0 \tag{12}$$

Thus, using the constitutive relations for linear Kirchhoff materials, the forces and moments of contact are given according to the linear and angular deformations, respectively (Cao et al., 2006). Thus, one can obtain a highly nonlinear system in terms of forces and moments of contact. Note that this system of equations can not be solved through direct integration. Therefore, the perturbation method was employed to obtain an approximate solution (Arfken et al., 2000). Importantly, these shift functions obtained from the static equilibrium are then used in dynamic analysis, which eliminates one of the major problems commonly found in classical techniques of finite elements, which is conveniently define the shape functions.

By associating the shape functions with the extended Hamilton principle is possible to find the Lagrange equations, which constitute a very elegant way to obtain the equations of motion of dynamical systems. In this work, we chose to omit the mathematic demonstration of these relations, which was presented in a straightforward manner, by Eq. (13), elementary equation of motion. The contour conditions, as well as the global equations of the systems, are mounted using they are mounted the similar form the classic theory of finite elements. More details about this implementation and the construction of the global matrix of the system can be found in the work of Cao (2005).

$$\mathbf{M}^{(e)}\ddot{\mathbf{q}}^{(e)}(t) + \mathbf{K}^{(e)}\mathbf{q}^{(e)}(t) + \mathbf{g}^{(e)}\left(\mathbf{q}^{(e)}(t)\right) = \mathbf{f}^{i(e)}(t) + \mathbf{f}^{c(e)}(t) + \mathbf{f}^{d(e)}\left(t, \mathbf{q}^{(e)}\right), \tag{13}$$

where $\boldsymbol{M}^{(e)}$ is the mass matrix, $\boldsymbol{K}^{(e)}$ is the linear stiffness matrix, $\boldsymbol{g}^{(e)}(\boldsymbol{q}^{(e)})$ is a nonlinear vector with quadratic an cubic terms on the components of $\boldsymbol{q}^{(e)}$and $\boldsymbol{q}^{(e)}$is the nodal displacement vector. The integration method used in the simulations is the Newmark method with imposition of conservation of mechanical energy, proposed by Bathe (2007).

### 2.4. Fluid-structure interaction

This section has been defined the methodology used to coupled the fluid and structural domain. Note that the mesh in these two domains is different, as illustrated in Figure 4), which states the mesh discretization of the fluid in rectangular elements arranged on the surface of a cylindrical structure and the mesh discretization of the structural domain, that the according to the theory of Cosserat formed by nodes positioned about a line.

A major problem faced in this stage is how to transfer forces and moments applied by the fluid on the surface of the cylinder, calculated by immersed boundary method, to the nodes of the mesh structure. This issue must also be resolved in the opposite direction, thus transferring the displacements, velocities and accelerations are calculated using the theory of Cosserat beam to the surface of the cylinder that will be in contact with the fluid.

The procedure adopted is to consider "slices" of the cylindrical mesh, in the length direction of the immersed cylinder, composed of a row of elements in the direction "z" and attach it to a given nodal point of the mesh structure, so that the force as well as the moment applied on the node of the structure mesh, are the result of demands imposed on all nodes in the mesh of fluid on the surface of the "slice" of the cylinder.

In Fig. (4), the red point represents the Lagrangian point of the submerged structure and the green point represents the node of the mesh structure. To accomplish the transfer of information between the two domains becomes necessary to use auxiliary axis of references. In this modeling were used three axes, which are shown in Figure 3), two of them mobile (*Axyz*) and ($Ax_1y_1z_1$) and a fixed (OXYZ). Thus using the concepts of kinematics and dynamics of three-dimensional

motion of a rigid body, forces and moments can be transferred from the surface of the cylinder immersed into the structure nodal point, and in reverse, transferring the displacement and velocity of the structural nodal point to surface immersed. Please note that the solution algorithm coupled, fluid-structure, is made using a partitioned method, thus solving one of the domains, either fluid or structural, is used as input in subsequent domain.

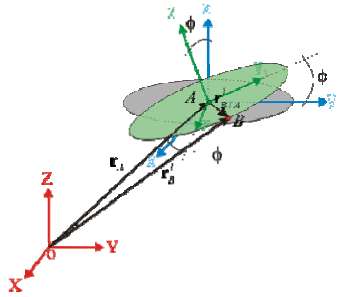


Figure 3. Sketch of cylinder slice and reference axes.

The Cosserat theory beans is used coupled with immersed boundary method to obtain the structural dynamic reaction support by excitation forced for the flow. For understand the fluid-structure interaction using the partitioned algorithm it is purposed the following steps:

1) Transport Eulerian equations of momentum are solved (eq.6), yielding the temporary parameter ($u_i^*$);

2) The temporary parameter ($u_i^*$) is interpolated to the Lagrangian domain;

3) The Lagrangian force, $F(\vec{x}_k, t)$ is evaluated (eq. 7). It noteworthy that in this case the velocity $U_{FI}$ is the structure velocity given also by the Cosserat theory;

4) As commented before, the displacements, velocity and acceleration of the structure are evaluated over a line positioned at the centroid of the immersed body, therefore it is necessary to evaluate the sum of the Lagrangian forces, $\sum_{nl} F(\vec{x}_k, t)$ and torque, $\sum_{nl} \vec{T} = \vec{r}\mathrm{x}\vec{F}$, (being $\vec{r}$ is the distance between lagrangian point and a node of structure center line) at such a line. Figure 4) exemplifies this procedure;

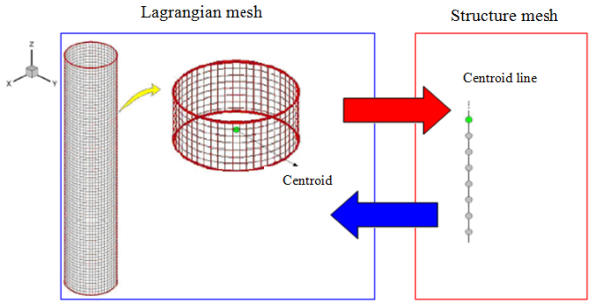


Figure 4. Coupling between the fluid and structural meshes.

5) The force evaluated at each Lagrangian point if $\mathrm{F_i}(\vec{\mathrm{x}}_\mathrm{k}, \mathrm{t})$ smeared over the Eulerian domain, yielding the Eulerian force, $\mathrm{f_i}(\vec{\mathrm{x}}, \mathrm{t})$;

6) The Eulerian velocity field is updated (eq. 8);

7) The Poisson equation is solved and the velocity field is updated with the pressure correction, finalizing the pressure-velocity coupling;

8) The sum of the Lagrangian forces and torque (calculated in forth step) is evaluated and a new position and velocity of center line structure, consequently the new positions of the Lagrangian points, are given;

9) Return to step (1).

## 3. Results

In this section we show the results of the simulations carried out for both validation of the numerical code, and of the simulation of flexible structures subject to cross flow. The effects of different Reynolds numbers ( $\mathrm{Re} = \rho UD/\mu$ , where $U$ is the uniform velocity imposed inlet and $D$ is diameter of cylinder) are assessed.

The eulerian domain has dimensions 30x20x10 in directions X,Y,Z, respectively, the base of cylinder is positioned in 10x10x0, in relation to coordinate axes OXYZ. For all simulations carried in this work the cylinder has a diameter *D=1.0* and a length *L=10.0*, as show in Figure 5).

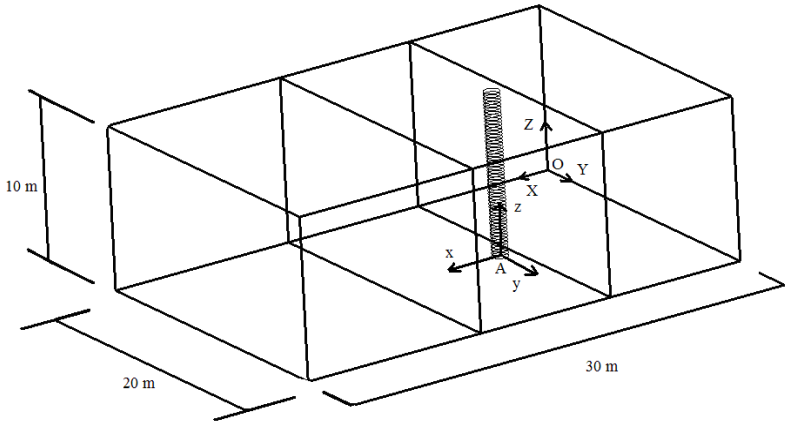


Figure 5. Eulerian and lagrangian domains.

The boundary conditions for the Eulerian domain flow in the plane X=0 is a uniform inlet profile $U_\infty$=1.0 [m/s] and at plane X=30 the advective boundary conditions is imposed. For other boundary conditions (planes Y=0, Y=20, Z=0 and Z=10) no-slip boundary conditions is imposed. All simulations used a cartesian uniform mesh divided in three parallels sub domains, (Vedovoto, 2009).

### 3.1. Rigid structure

In order to validate the flow solver, the first simulations are performed without move the cylinder at different Reynolds numbers. Drag (*Cd*) coefficient and Strouhal numbers are compared with the data provided by White (1991) and shown in Table 1). The differences between Strouhal number present in Table 1) is probably due the proximity of boundary conditions of the cylinder and the length of cylinder.

Table 1. Comparison among different Reynolds numbers for drag coefficient and Strouhal number.

| | *Re=100* | | *Re=500* | | *Re=1000* | |
|---|---|---|---|---|---|---|
| | Cd | St | Cd | St | Cd | St |
| *White (1991)* | 1.40 | 0.18 | 1.30 | 0.21 | 1.10 | 0.21 |
| *Present work* | 1.51 | 0.14 | 1.31 | 0.16 | 1.30 | 0.16 |

### 3.2. Flexible structure

The flexible structure is modeled by the Cosserat theory of slender beams. The hydrodynamic forces required by such a methodology are provided by the immersed boundary method. Three different values of Reynolds number were studied (Re= 100, 500 and 1.000). The physical and geometrical properties of the flexible cylinder are given in Tab. (2).

Table 2. Physical and geometrical properties of the flexible cylinder.

| **Properties** | **Values** |
|---|---|
| Aspect ratio (L/D) | 10 |
| Density | 7850 [Kg/m$^3$] |
| Axial stiffness(EA) | 5,014x10$^4$ [N] |
| Bending stiffness(EI) | 907,53 [Nm$^2$] |
| Torsion stiffness (GJ) | 682,55 [Nm$^2$/rad] |

As boundary conditions for the structure model, revolute joints are adopted and hence displacements both the extremities and the torsional degrees-of-freedom were eliminated, allowing however, rotation in the directions x and y. The immersed structure is discretized using 50 Cosserat elements equally spaced, with 51 nodes and 6 degrees of freedom by node.

The fig.(7) displays two snapshots of the flow past a flexible cylinder ate t= 860s (left) and t=875 s (right) ate Re=1000. Due to structural stiffness, and the magnitude of hydrodynamic forces imposed by flow, was not observed a visual deformation of the structure in this case, however, as will be shown in later figures, there is a variation in structural position within the flow, although not sufficiently to affect the large fluid structures of the flow around.

It is observed in Fig. (7) the Von Karman wake, characterized by the periodic vortex shedding (which is responsible for exciting the structure in the direction transverse to the flow).

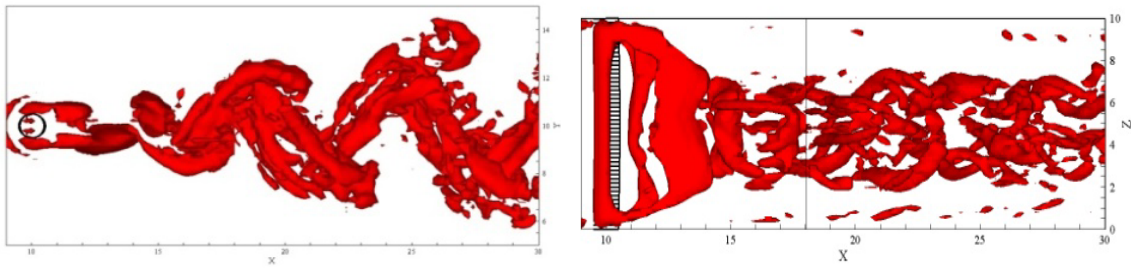


Figure 6. Coherent fluid structures downstream the immersed cylinder. Iso-surfaces of Q=0.25.

For a quantitative evaluation of the flows here simulated Fig. (8) shows the drag and side coefficients. Although the movement of the flexible structure is not visibly notable considering the characteristic dimensions involved in the simulations its influence is undeniable when drag and side coefficients are analyzed.

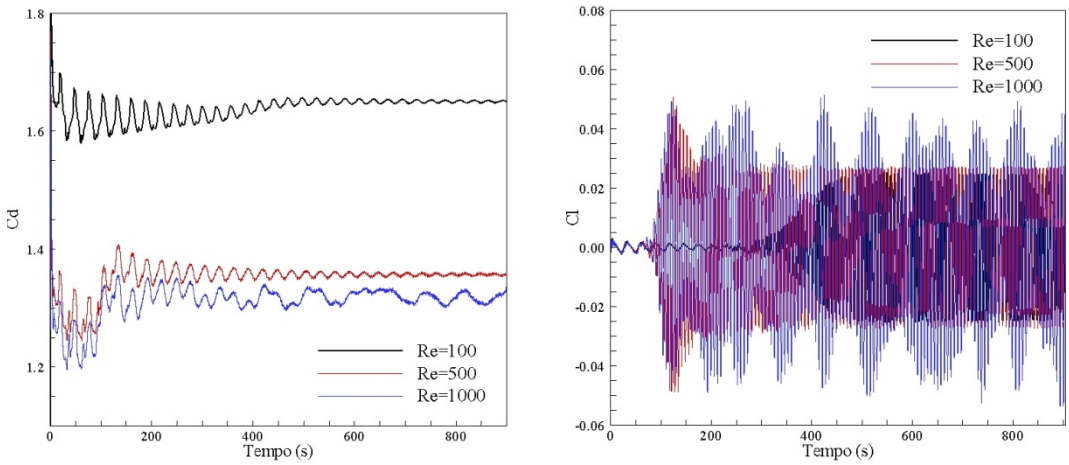


Figure 8. Drag (left) and side (right) coefficients of the flexible structure.

In Fig. (8) is noteworthy the effect of the Reynolds number in the quantitative coefficients. Since a higher Reynolds number implies in higher efforts over the structure is natural an increase in the values of displacements of the flexible body. This phenomena promotes thus a higher oscillation of the signals, especially for Reynolds number higher than 500.

Considering the analysis of the data provided by the structural model by the simulations, Fig. (9) suggests that the affirmation of the last paragraph is physically consistent. In this figure the evolution in time of the displacement of a nodal point positioned at the Z= 4.80 m from the bottom of the domain can be observed.

It is observed in Fig. (9) (left), in which all values of Reynolds numbers are considered, the shift toward normal direction shows an exponential decay, typical of viscous damping. It is worthy to note that the observed damping is due entirely to the fluid-structural interaction, because the structural model was not considered any damping inherent in the material.

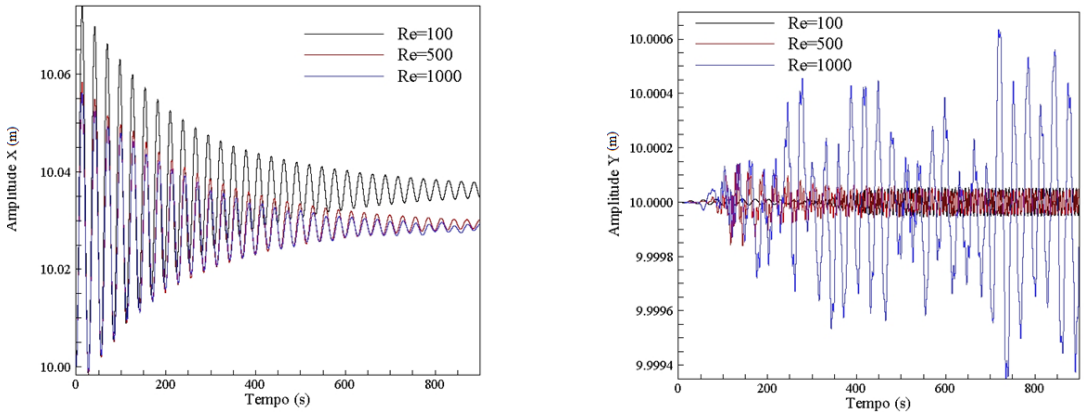


Figure 9. Flexible Structure subject to flow at different Reynolds numbers: Time history of displacement in direction (left) X, (right) Y.

In Fig. (9) (right) we show the evolution of the displacement of the same nodal point in the transverse direction Y. One can note that the transverse displacement increased significantly for Re = 1000 due a higher influence of turbulence, i e. an increase of the vortex shedding downstream of the cylinder, that consequently, alters the pressure field and hence the hydrodynamic forces that structure are submitted.

Fig. (10) presents the structural shifts of the line of centroids of the flexible structure subject to flow for Re = 1000.

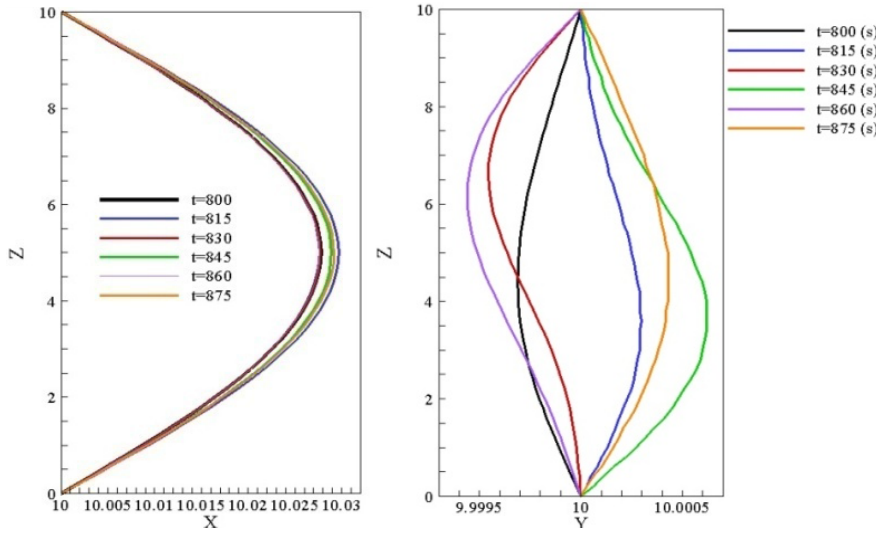


Figure 10. Displacements of the centroid line.

In Fig. (10) one notices the differences between the structural shifts in the longitudinal and transverse direction. The longitudinal displacement due to drag force causes the structure to move up to certain position and oscillate around it. Unlike the lateral force, this causes the structure to oscillate around zero, according to the vortex shedding in a combination of frequencies. As previously reported, this phenomenon is known as VIV (Vortex-Induced Vibration). It is noteworthy also that the longitudinal displacement was larger than the cross for this simulation.

## 4. CONCLUSION

We present a new approach for FSI problems applied to flexible cylinders. This promising approach is better detailed in work of Borges (2010) and Vedovoto (2009), allowing to solve problems with large deformations. It is a major area of interest of the oil industry.

The Cosserat theory and immersed boundary method enabled to simulate a full FSI problem, which the structure movement is produced just by fluid flow forces. While all characteristics of flow, laminar or turbulent, are preserved. New simulations are been performed to obtain large aspect ratios, for this aspects as code parallelism are being implemented.

## 5. ACKNOWLEDGEMENTS

The authors thank the College of Engineering Mechanical (FEMEC) of the University Federal of Uberlândia (UFU), Capes, FAPEMIG and CNPq for financial support.

## 6. REFERENCES

Antman S.S. Nonlinear Problems of Elasticity, Applied Mathematical Sciences. 2.ed. New York: Springer-Verlag, 1995. 884p.

Arfken, G.; Weber, H. J.; Harris, F. Mathematical Methods for Physicists. 5.ed. Academic Press Inc., San Fiego. 2000. 1112p.

Argyris, J.H.; Dunne, P.C.; Malejannakis, G.; Scharpf, D.W. On large displacements–small strain analysis of structures with rotational degree of freedom. Computer Methods in Applied Mechanics and Engineering. v.14, p.99-135, 1978.

Baarholm, G.S.; Larsen, C.M.; Lie, H. On fatigue damage accumulation from in-line and cross-flow vortex-induced vibrations on risers. Journal of Fluids and Structures. v. 22, p. 109-127. Jan. 2006.

Bathe, K.J. Conserving Energy And Momentum In Nonlinear Dynamics: A Simple Implicit Time Integration Scheme. Computers and Structures. v.85, p. 437–445. 2007.

Borges, A.S. Desenvolvimento de procedimentos de modelagem de interação fluido- estrutura combinando a teoria de vigas de Cosserat e a metodologia de fronteira imersa. 2010. 199 f. Tese de Doutorado, Universidade Federal de Uberlândia, Uberlândia, MG.

Cao, D.Q.; Dongsheng, L.; Charles, H.; Wang, T. Nonlinear dynamic modelling for MEMS components via the Cosserat rod element approach. J. Micromech. Microeng. v. 15, p. 1334–1343. 2005.

Cao, D. Q.; Dongsheng, L.; Charles, H.; Wang, T. Three Dimensional Nonlinear Dynamics Of Slender Structures: Cosserat Rod Element Approach. International Journal of Solids and Structures. v. 43, p. 760-783. 2006.

Griffith, B.E. and Peskin, C.S., 2005, "On the order of accuracy of the immersed boundary method: higher order convergence rates for sufficiently smooth problems", Journal Computational Physics, Vol.208, pp. 75-105.

Lima e Silva, A., Silveira-Neto, A. and Damasceno, J., 2003, "Numerical simulation of two dimensional flows over a circular cylinder using the immersed boundary method", Journal of Computational Physics, Vol.189, pp. 351–370.

Mariano, F.P., Moreira, L.Q., Silveira-Neto, A., da Silva, C.B. and Pereira, J.C.F., 2010, "A new incompressible Navier-Stokes solver combining Fourier pseudo-spectral and immersed boundary methods", Computer Modeling in Engineering Science, Vol.1589, pp. 1-35.

Uhlmann, M., 2005, "An immersed boundary method with direct forcing for the simulation of particulate flows", Journal of Computational Physics, Vol.209, pp. 448-476.

Vedovoto, J.M., Desenvolvimento de uma modelagem da combustão em escoamento turbulento baseada em metodologia híbrida euleriana/lagrangiana e na metodologia da fronteira imersa. Uberlândia: UFU, 2009. 124 f. Relatório de qualificação para o doutorado em Engenharia Mecânica.

Wang Z., Fan J. and Luo, K., 2008, "Combined multi-direct forcing and immersed boundary method for simulating flows with moving particles", International Journal of Multiphase Flow, Vol.34, pp. 283-302.

WHITE, F. M. Viscous fluid flow. 2. ed. New York: McGraw-Hill, 1981. 614p.

## 5. RESPONSIBILITY NOTICE

The authors are the only responsible for the printed material included in this paper.